Journal of Asian Ceramic Societies

ISSN: (Print) (Online) Journal homepage: https://www.tandfonline.com/loi/tace20

Production of Si_3N_4 porous beads via carbothermal reduction and nitridation technique

Gülsüm Topateş & Ayse Kalemtaş

To cite this article: Gülsüm Topateş & Ayse Kalemtaş (2020) Production of Si_3N_4 porous beads via carbothermal reduction and nitridation technique, Journal of Asian Ceramic Societies, 8:4, 1197-1205, DOI: 10.1080/21870764.2020.1833415

To link to this article: https://doi.org/10.1080/21870764.2020.1833415

Published online: 16 Oct 2020.

JOURNAL OF ASIAN CERAMIC SOCIETIES
2020, VOL. 8, NO. 4, 1197–1205
https://doi.org/10.1080/21870764.2020.1833415

THE CERAMIC SOCIETY OF JAPAN
THE KOREAN CERAMIC SOCIETY
Taylor & Francis
Taylor & Francis Group

FULL LENGTH ARTICLE

Production of Si_3N_4 porous beads via carbothermal reduction and nitridation technique

Gülsüm Topateş [a] and Ayse Kalemtaş [b]

[a]Department of Metallurgical and Materials Engineering, Ankara Yıldırım Beyazit University, Ankara, Turkey; [b]Department of Metallurgical and Materials Engineering, Bursa Technical University, Bursa, Turkey

ABSTRACT

Si_3N_4 porous beads were produced from direct carbothermal reduction and nitridation of spheres composed of carbon+SiO_2 mixtures. A simple one–step sol–gel templating technique was used to prepare carbon+SiO_2 (molar ratio of carbon/SiO_2 was set as 4) containing spheres with a diameter of 2 mm. A natural and abundant biopolymer, alginate, is used as a sacrificial template to produce porous Si_3N_4 ceramic beads. Carbothermal reduction and nitridation process was conducted at two different temperatures (1500 and 1550°C) and atmospheres (pure nitrogen and 5% hydrogen in nitrogen) to observe the effect of process parameters on the yield of Si_3N_4. Porous beads with a smooth shape and without any deformation were successfully obtained after the carbothermal reduction and nitridation process. X–ray powder diffraction studies showed that the use of H_2 increased the amount of Si_3N_4 formed by accelerating the reduction and nitridation reactions. Microstructural investigations revealed oxide addition changed grain morphology from fiber–like to short, angular geometry. This microstructural development showed that the addition of oxide powder increased the amount of liquid phase formed during the heat treatment process and changed carbothermal reduction and nitridation mechanism from vapor–solid to vapor–liquid solid.

ARTICLE HISTORY
Received 24 June 2020
Accepted 1 October 2020

KEYWORDS
Sol–gel templating; carbothermal reduction–nitridation; porous Si_3N_4 beads

1. Introduction

Porous oxide and non–oxide ceramics can be fabricated via various techniques such as gel casting [1–5], freeze–casting [6–8], partial sintering [9–14], foaming [15,16], 3D printing [17–19], replica [20–23], and using fugitive additives [9,12,24–26] etc. Carbon black [27–29], starches [9,21,30], sawdust [31,32], and some other fugitive materials are used to provide high open porosity content and enhance achieving highly interconnected porosity. Adjusting the pore amount, as well as pore size and distribution, is a challenging task for the production of porous ceramics.

In the last decade, porous and poly–hollow ceramic microspheres have recently been subjected to systematic research to produce porous oxide and non–oxide ceramics [33–36]. Poly–hollow ceramic spheres can facilitate controlling the porosity amount, pore size and size distribution, and pore morphology of the porous ceramics. Also, the type of porosity, open or closed porosity, can be managed by the usage of the porous or poly–hollow ceramic spheres as a reinforcement for the production of porous ceramics or composites, respectively. Valorization of porous and hollow ceramic spheres for the fabrication of porous ceramics is a challenging issue, but porous micro and nano–ceramic spheres are known for a long while and have a wide application area. Owing to their unique characteristic properties such as low density, high porosity, ample interior space, high surface area, a mechanically and thermally stable structure, high and reproducible performance, and providing an opportunity to use economical materials, hollow and porous ceramic and composite spheres have various applications [37–39]. It is also possible to achieve hierarchically porous structures via various production techniques, and it is possible to tailor the interior and exterior surface of the spheres to design the microstructure depending on the desired application area. The spherical shape of these porous structures provides many favorable properties such as flowability, very good mobility, and high packing efficiency [40]. Ceramic and composite spheres can be used for various applications in biomedical areas such as hard tissue regeneration, cement, drug delivery, delivery of antibiotics, protein delivery, bioreactors, and can be used as filler or packing materials in many biomedical applications [41]. Also, these porous ceramic spheres can be used for numerous applications such as insulation, radiant burners, catalyst support, adsorption–separation, solar cells, filters, sensing devices, wastewater treatment, energy storage, pigments, coatings, thermostable materials, and as reinforcement for foams for the structural applications [42–46]. These micro and nano–ceramic spheres have been used in many industrial applications in combination with different types of materials.

Fabrication of hollow/porous ceramic spheres is carried out via various processing techniques such as sacrificial core [47–49], spray drying [50–53], solvothermal

CONTACT Gülsüm Topateş gtopates@ybu.edu.tr

process [54–58], nozzle reactor and microwave–assisted solvothermal synthesis [59], soft (templating vesicles, emulsions, micelles, etc.) and hard (templating silica, carbon, etc.) templating [45,60–67], multi–template [68], sol–gel templating [69–71], pseudomorphic synthesis [72], cathode plasma electrolysis [73], hydrothermal processing [74–77], emulsion microencapsulation [78], sonochemical [68], and emulsion evaporation [53,79].

It is well known that carbothermal reduction–nitridation (CRN) of SiO_2 is an attractive method to manufacture Si_3N_4 powders with controlled grain morphology. Use of natural starting materials, relative lower CRN temperatures and possibilty of tailoring final Si_3N_4 powder make CRN one of the prevalent methods used during the fabrication of Si_3N_4. Formation of Si_3N_4 via CRN reaction takes place in two steps; 1. SiO_2 source is reduced into SiO that is in gaseous form, 2. this SiO is nitrided into Si_3N_4 by the presence of carbon. The CRN technique has been extensively studied for the production of Si_3N_4 powder [80–84]. Limited studies have shown the potential of CRN for the production of bulk Si_3N_4 ceramics. Li et al. successfully obtained porous Si_3N_4 ceramic tubes by carbothermal reduction of diatomite preforms [84]. Topateş showed Si_3N_4 foams can be produced by a combination of CRN and replica techniques [23]. Zhao et al. prepared Si_3N_4 hollow microspheres by using the template method combined with the CRN method [66,80–83,85]. In this study, sodium alginate is used as an in situ gelling templates to produce SiO_2+ carbon containing millimeter–sized macrobeads. Designed porous Si_3N_4 beads were achieved via direct CRN of sodium alginate+SiO_2+ carbon containing macro beads at 1500 and 1550°C for 5 hours at two different sintering atmosphere conditions. This study is going to be the first work in the literature carried out on the production of porous macro Si_3N_4 beads with mm–size via in situ gelling templates followed by a CRN of sodium alginate+carbon+SiO_2 containing macro beads.

2. Experimental procedure

SiO_2 (Ege Nanotek Ltd., Turkey; average particle size: 10 µm) and carbon (Isaf N 220, Tüpraş Co., Turkey; surface area: 112 m^2/g) sources were mixed with a molar ratio of carbon/SiO_2 was set to 4. To observe the effect of additives on CRN process, 5 wt. % of Y_2O_3 (H.C. Starck Berlin) was used. Homogeneous slurries were obtained by ball mill (MSE Technology, Turkey) at a speed of 160 rpm with Si_3N_4 balls for 24 h. The slurries were dried in a rotary evaporator and the sieved through a 125 µm screen.

SiO_2 and carbon containing bead production was performed via the following steps. Three grams of sodium alginate (Katki Dunyası, Turkey) was dissolved in 100 mL distilled water by stirring overnight at room temperature. A homogenous slurry containing 4.7 g SiO_2+ carbon mixture and 100 mL sodium alginate solution was prepared in a planetary ball mill at a rotation speed of 350 rpm for 30 minutes. The cross-linking calcium chloride ($CaCl_2$) solution was prepared by mixing 1.0 g of $CaCl_2$ (Katki Dunyası, Turkey) in 100 mL distilled water by magnetic stirring at room temperature for 1 hour. Prepared aqueous sodium alginate+SiO_2+ carbon solution was added dropwise into $CaCl_2$ aqueous solution at room temperature using a 60 mL hypodermic syringe through a needle under constant stirring at room temperature. The alginate–ceramic composite beads are formed via cross-linking in the $CaCl_2$ solution for at least hour (Figure 1). Then beads are removed from the solution via sieving and washed with distilled water for many times. Macroscopic investigations depicted that spherical millimeter–sized sodium alginate+SiO_2+ carbon containing macrobeads were fabricated.

Sodium alginate, a natural polymer, was used as an in–situ gelling template to produce designed spherical porous ceramic macro beads. The sodium alginate's thermal behavior was investigated by thermogravimetric–differential thermal analysis (TG–DTA) (TA, SDT650) between 20–1000°C under a nitrogen atmosphere with a heating rate of 10°C/min.

Prepared spheres were placed into Al_2O_3 crucible and heat treated in Al_2O_3 tube furnace (MTI GSL–1700X–II, USA) under two different atmospheres (% 99.99 nitrogen and %95 nitrogen+%5 hydrogen) and temperatures (1500 and 1550°C). The applied heating rate was 7°C/min and duration was 5 hours. The composition and heat treatment parameters of the spheres were summarized in Table 1. Higher carbon+SiO_2 ratio that accelerates the CRN rate via enlarging the contact area between carbon and silica particles formed excess carbon after CRN reaction. This excess carbon was burned in an air atmosphere at 700°C for 4 h.

After the heat treatment process, X–ray diffraction (XRD) (Rigaku MiniFlex–600, Japan) examination was done for all spheres. Spheres were ground in an agate mortar and sieved through a 63 µm screen before XRD analysis. Scanning electron microscope (SEM) (Hitachi SU–500, Japan) equipped with X–ray energy dispersive spectroscopy was used to observe the microstructural development.

3. Results and Discussion

3.1. Phase development of Si_3N_4 beads

Sodium alginate is a natural biopolymer, and in the current work, it was used as a template to achieve designed ceramic beads via the sol–gel process. Figure 2 reveals TG, DTA, and DTG curves for the sodium alginate. TG curves depicted that sodium alginate began to lose weight just after 35°C, and the weight loss reached 100% at lower than 900°C under nitrogen atmosphere.

Figure 3. shows the XRD patterns of Si_3N_4 beads without Y_2O_3 addition. For composition A1 and A2, α–Si_3N_4

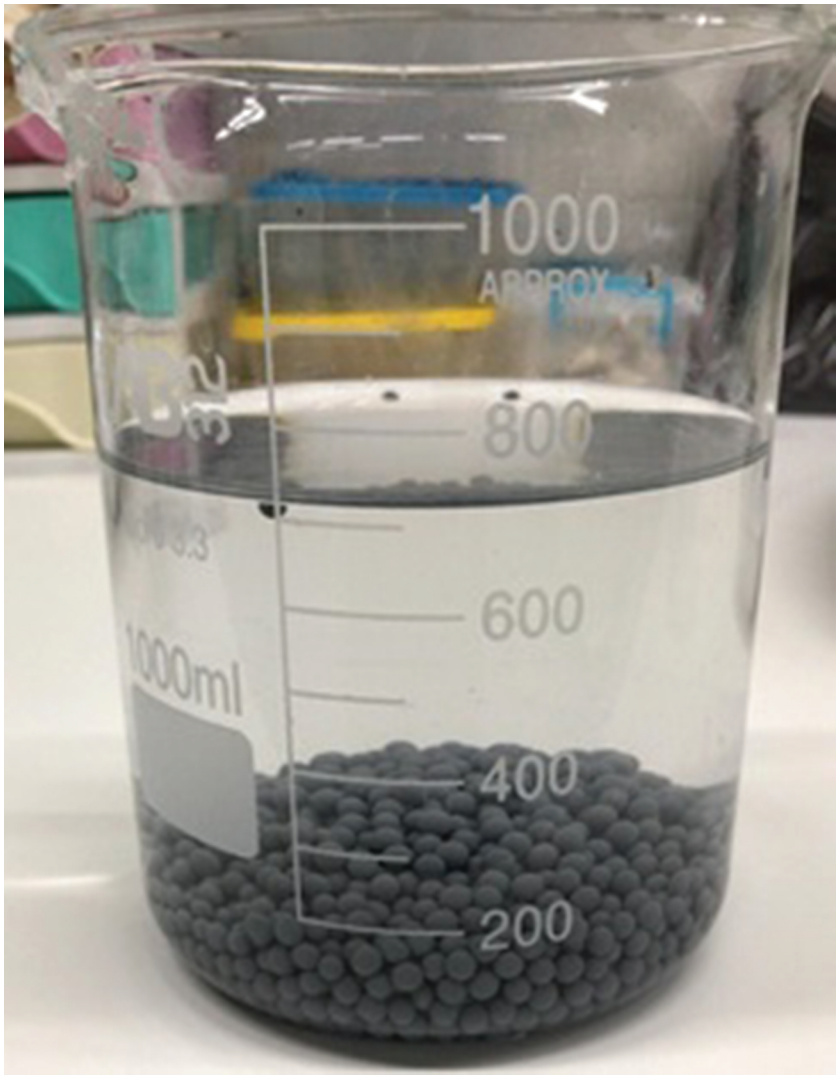

Figure 1. Fabricated sodium alginate+SiO_2+ carbon containing beads in $CaCl_2$ aqueous solution.

Table 1. Compositions and heat treatment conditions of beads used in the study.

Bead	SiO_2 (wt. %)	Carbon (wt. %)	Y_2O_3 (wt. %)	Atmosphere	CRN temperature (°C)
A1	55.56	44.44	–	N_2	1500
A2	55.56	44.44	–	N_2	1550
A3	55.56	44.44	–	N_2+ H_2	1550
B1	55.56	44.44	5	N_2	1500
B2	55.56	44.44	5	$TabN_2$	1550
B3	55.56	44.44	5	N_2+ H_2	1550

and SiC are the two major phases obtained. Higher temperatures (>1450°C), the presence of impurities, the addition of free Si and lower nitrogen pressure are the results of the formation of undesirable SiC phase [85]. At high temperatures, Si_3N_4 becomes unstable, as the nitrogen pressure isn't sufficient, SiC formation is being observed [85].

Besides these phases, unreacted SiO_2 is also present in the samples that show the CRN yield was lower. The effective parameters on the efficiency of CRN reaction are carbon to SiO_2 ratio, crucible design, nitrogen pressure, the particle size of starting powders, oxide additives, etc. To obtain a higher yield of Si_3N_4, the contact between carbon and SiO_2 should be perfect. Increased contact promotes the formation of SiO gas that is the first step of Si_3N_4 formation. The use of excess carbon than the stoichiometric amount of CRN is the one approach to increase the contact area of starting powders [81]. Therefore, higher carbon amounts have been selected for the complete reduction of SiO_2. Arık et al. [86] studied various carbon/SiO_2 ratios from 1.5 to 7.5. For the lowest ratio, some amount of sepiolite was detected. When the ratio increased to 4, they detected some amount of C that shows the conversion of SiO_2 was fulfilled [86]. In another study, the yield of Si_3N_4 increased from 20% to 90% as the carbon to SiO_2 ratio doubled from 2 to 4. The design of crucible was also investigated in the

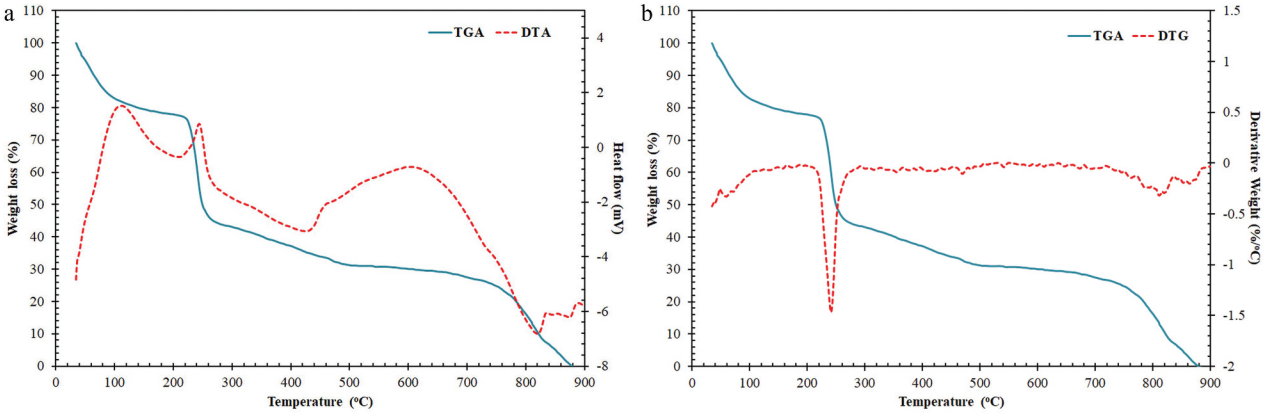

Figure 2. (a) TG–DTA and (b) TG–DTG curves for the sodium alginate under nitrogen atmosphere.

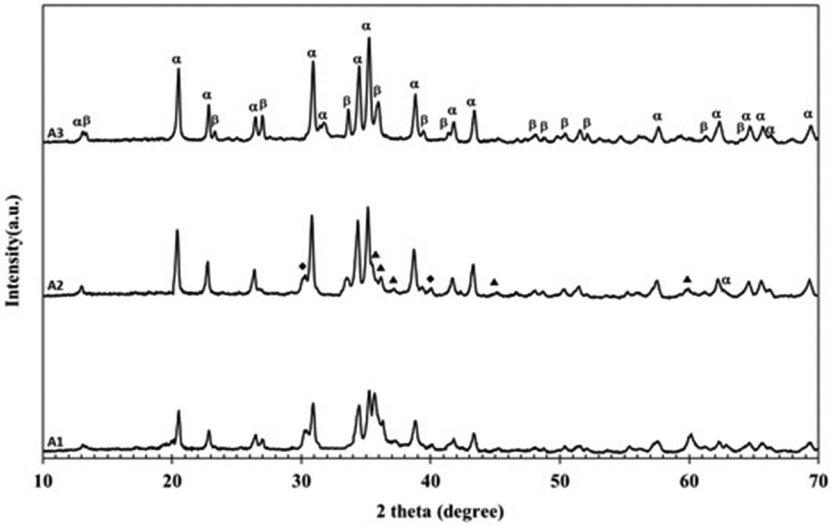

Figure 3. XRD measurements of Si_3N_4 beads without Y_2O_3 addition (**α**: α–Si_3N_4,: β–Si_3N_4,:SiO_2: SiC).

same study. Graphite crucible with holes at the bottom and pure alumina crucible without holes were used. The holes enabled the flow of nitrogen through the powders, removal of CO gas, and further proceedings of the CRN reactions. Conversely, gaseous products were concentrated in Al_2O_3 crucible due to a lack of nitrogen flow and reduced the yield of Si_3N_4 around 10% [81]. Even a higher ratio was selected in this study, the use of non–perforated Al_2O_3 crucible during the CRN of spheres can be the reason of unreacted SiO_2. The poor nitrogen flow and accumulation of products of the CRN process may shift the reaction left for A1 and A2. The other reason for lower reaction efficiency can be the larger particle size of starting powders. Shan et al. investigated the effect of particle size by milling SiO_2 powder for various hours. Increasing milling time reduced the particle size of SiO_2 from 100 µm to 10 µm, enhanced the CRN process, and produced finer β–grains [87].

Several studies used a gas mixture of N_2+ H_2 to accelerate the CRN rate. To increase the reaction yield, the CRN process was conducted under N_2 + H_2 for A3. SiO_2 and SiC phases disappeared, the formation of β–Si_3N_4 was observed. Even though the use of hydrogen isn't thermodynamically favored owing to higher partial pressure, the higher mobility of hydrogen removes this disadvantageous situation. Rahman and Riley increased the extent of nitridation from 20% to 55% after changing the atmosphere to N_2+ H_2.

Oxide additives contribute to the formation of a liquid phase, and this liquid phase changes the Si_3N_4 formation from vapor–solid transport to vapor–liquid–solid transport. α–Si_3N_4 is nucleated from SiO vapor, while β–Si_3N_4 forms from the deposition of SiO in the liquid phase and supersaturation of β phase in this liquid. The addition of Y_2O_3 into the starting mixture promotes the formation of the liquid phase during the CRN process. As given in Figure 4, higher amount of β–Si_3N_4 was generated with a small amount of α phase. Also, $Y_4Si_2O_7N_2$ was detected as the secondary phase.

3.2. Microstructural development of Si_3N_4 beads

Figure 5 (a,b) illustrate the size and morphology of beads before and after the CRN process. A smooth sphere bead was produced from a carbon and SiO_2 mixture with a diameter of 2.10 mm. The calculated shrinkage value for B3 is 17% after CRN, some deformation was observed on the beads due to this shrinkage. The solid inner structure of the bead can be seen from Figure 5 (c). Fibers were generated on the surface of the bead from A3, as seen in Figure 5 (d). The length of fibers varied between 200 µm composed of α–Si_3N_4 from XRD given in Figure 3.

The detailed microstructural investigations of beads were carried out, and the images were given between Figure 6 (a)–(d). Very fine and isometric grains were produced for bead A1 (Figure 6 (a)). Grains were agglomerated and lose packing of these agglomerates produced a porous structure. The morphology of grains differed as the parameters of CRN changed. Increasing temperature and use of hydrogen in the CRN atmosphere resulted in the formation of fiber–like grains in A3 (Figure 6 (b)). The width of the fibers was the submicron size, and the length was between 200 µm. Rahman and Riley used the N_2+ H_2 atmosphere during the CRN process of rice husk. They produced α phase with whisker form and concluded that coarser starting powder promoted the formation of whiskers [88]. Also, this grain shape suggested generation of Si_3N_4 took place via a typical vapor–solid mechanism [89]. As Y_2O_3 was added as additive oxide, the formation mechanism of Si_3N_4 changed from vapor–solid to vapor–liquid–solid. For B1, two types of grain shape were observed; fiber–like and fine, equiaxed grains

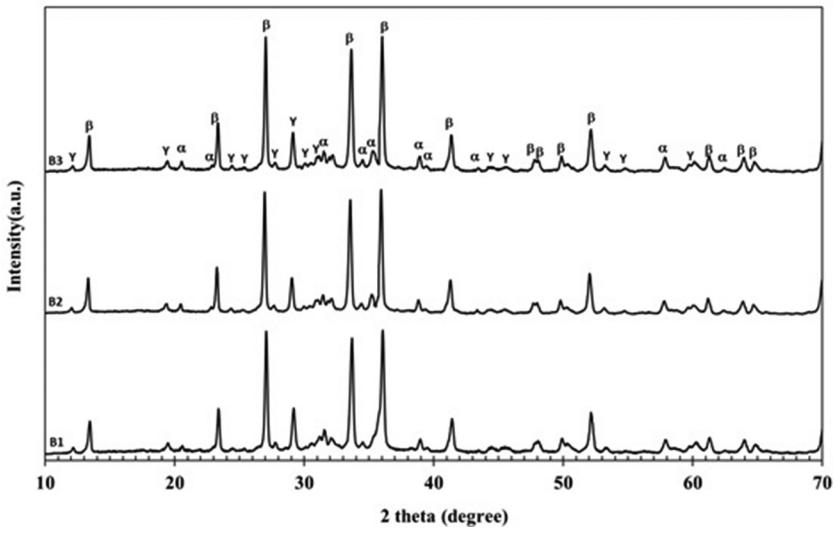

Figure 4. XRD measurements of Si_3N_4 beads with Y_2O_3 addition (**α**: α–Si_3N_4, **β**: β–Si_3N_4, **Y**: $Y_4Si_2O_7N_2$).

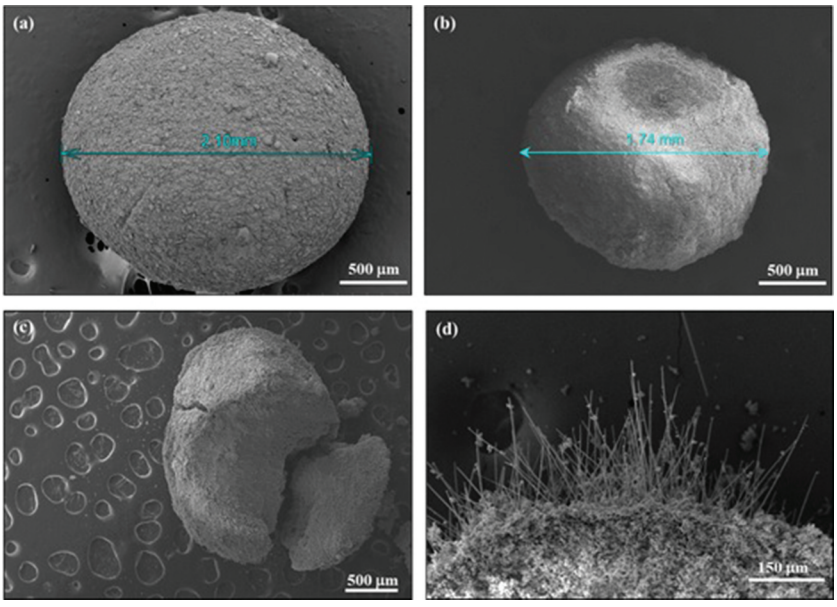

Figure 5. SEM images of beads (a) B before CRN, (b–c) B3 after CRN, and (d) formation of fibers in A3.

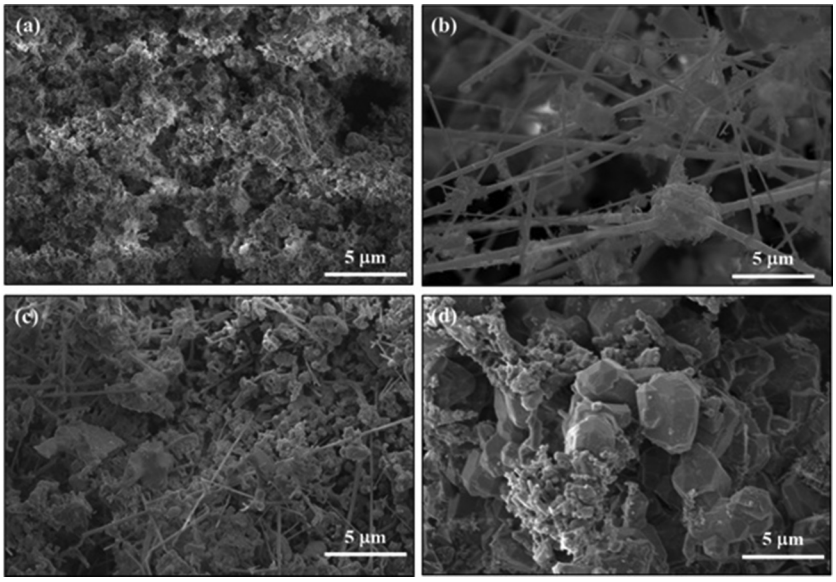

Figure 6. Microstructures of (a) A1, (b) A3, (c) B1, and (d) B3 beads.

in Figure 6 (c). Larger and hexagonal cross–sectioned Si_3N_4 grains were produced for B3 (Figure 6 (d)) after changing the temperature and atmosphere of CRN. Higher temperature induced the growth of β–grains and also some agglomerated structures due to the increased amount of liquid phase.

Compositional changes in B3 were further characterized by EDX as given between Figure 7 (a)-(c). As seen from the EDX data (Figure 7 (b)), the aggregates comprised Ca, O and Y besides Si and N. $CaCl_2$ used as cross–linking solution is the possible source for Ca entity. An excessive amount of liquid phase produced through the contribution of $CaCl_2$, this results coalescence of grains. On the other side, hexagonal, equiaxed grains formed individually (indicated by point 2) contained Si and N as major elements as given in Figure 7(c). C was also detected from both points due to the incomplete burn–out of excess carbon.

4. Conclusions

The sol–gel templating technique, using sodium alginate as a gel–forming biopolymer, followed by thermal treatment is, a facile technique for the preparation of millimeter–sized porous ceramic macro beads. In this study, designed porous Si_3N_4 beads were achieved via direct CRN of sodium alginate+SiO_2+ carbon containing macrobeads at 1500 and 1550°C for 5 hours at two different sintering atmosphere conditions. This study is going to be the first work in the literature carried out on the production of porous macro Si_3N_4 beads with mm–size via in situ gelling template followed by a CRN of sodium alginate+carbon+SiO_2 containing macro beads.

Porous Si_3N_4 beads with mm–size were successfully produced via CRN of carbon SiO_2 powder mixtures. CRN enabled a simple and cost–effective approach for fabrication. Inspite of higher shrinkage value,

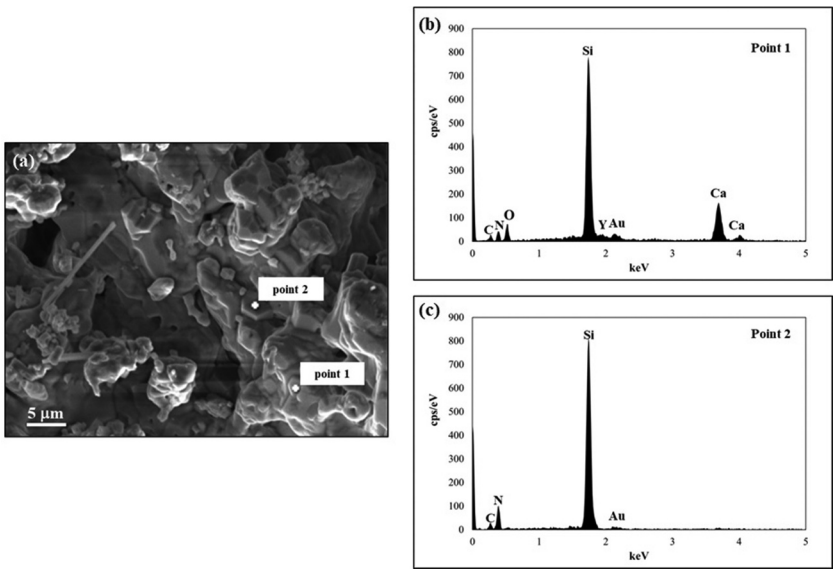

Figure 7. (a) SEM image and EDX spectra of (b) aggregate and (c) individual grains from B3 beads.

smooth beads with a solid inner structure was achieved.

CRN parameters and composition directly affected the yield of Si_3N_4 and morphology of grains. The pure nitrogen atmosphere reduced the reaction efficiency and caused SiC formation. Use of 5% hydrogen in nitrogen enhanced reactions and prevent SiC generation. Y_2O_3 has a positive contribution to the CRN process by promoting the formation of a liquid phase, a higher amount of β–Si_3N_4 produced by the supersaturation of grains from this liquid phase.

Porous Si_3N_4 beads can be promising materials for various applications such as implants, drug delivery, filtration, membrane, and sensing applications.

Disclosure statement

No potential conflict of interest was reported by the authors.

ORCID

Gülsüm Topateş http://orcid.org/0000-0003-4453-8219

References

[1] Li L, Wang H, Porous SS. Si_3N_4 ceramics prepared by TBA-based gel-casting. J Mater Sci Technol. 2015;31 (3):295–299.
[2] Yang X, Li B, Zhang C, et al. Design and fabrication of porous Si_3N_4-Si_2N_2O in situ composite ceramics with improved toughness. Mater Design. 2016;110:375–381.
[3] Brouczek D, Open-Porous Silicon KT. Nitride-Based Ceramics in Tubular Geometry Obtained by Slip-Casting and Gelcasting. Adv Eng Mater. 2017;19(10):1700434.
[4] Yin S, Pan L, Liu Y, et al. Effect of β– si_3N_4 seeds on microstructure and properties of porous Si_3N_4 ceramics prepared by gelcasting using DMAA system. Ceram Int. 2020;46(4):4924–4932.
[5] Yin S, Guo L, Pan L, et al. Porous fused silica ceramics prepared by gelcasting using multigrade fused silica powders. J Alloy Compd. 2020;819:152982.
[6] Deville S. Freeze-casting of porous ceramics: a review of current achievements and issues. Adv Eng Mater. 2008;10(3):155–169.
[7] Hu L, Wang C-A, Huang Y, et al. Control of pore channel size during freeze casting of porous YSZ ceramics with unidirectionally aligned channels using different freezing temperatures. J Eur Ceram Soc. 2010;30 (16):3389–3396.
[8] Han J, Hong C, Zhang X, et al. Highly porous ZrO_2 ceramics fabricated by a camphene-based freeze-casting route: microstructure and properties. J Eur Ceram Soc. 2010;30(1):53–60.
[9] Kalemtas A, Topates G, Özcoban H, et al. Mechanical characterization of highly porous β-Si_3N_4 ceramics fabricated via partial sintering & starch addition. J Eur Ceram Soc. 2013;33(9):1507–1515.
[10] Nanjangud SC, Brezny R, Green DJ. Strength and Young's modulus behavior of a partially sintered porous alumina. J Am Ceram Soc. 1995;78(1):266–268.
[11] Yang J-F, Zhang G-J OT. Porosity and microstructure control of porous ceramics by partial hot pressing. J Mater Res. 2001;16(7):1916–1918.
[12] Ohji T, Fukushima M. Macro-porous ceramics: processing and properties. Int Mater Rev. 2012;57(2):115–131.
[13] Gregorová E, Pabst W, Nečina V, et al. Young's modulus evolution during heating, re-sintering and cooling of partially sintered alumina ceramics. J Eur Ceram Soc. 2019;39(5):1893–1899.
[14] Uhlířová T, Nečina V, Pabst W. Modeling of Young's modulus and thermal conductivity evolution of partially sintered alumina ceramics with pore shape changes from concave to convex. J Eur Ceram Soc. 2018;38(8):3004–3011.
[15] Du, Z., Yao, D., Xia, Y., Zuo, K., Yin, J., Liang, H., Zeng, Y-P.. Highly porous silica foams prepared via direct foaming with mixed surfactants and their sound absorption characteristics. Ceram Int. 2020;49 (6):12942-12947.
[16] Jin, H., Yang, Z., Li, H., Jia, D., & Zhou, Y. Fabrication of Si2N2O Ceramic Foam by Combination of Direct Ink Writing and Biological Foaming Techniques. Adv Eng Mater.2020;22(4):1901541.
[17] Ma H, Feng C, Chang J, et al. 3D-printed bioceramic scaffolds: from bone tissue engineering to tumor therapy. Acta Biomater. 2018;79:37–59.
[18] Du X, Fu S, Zhu Y. 3D printing of ceramic-based scaffolds for bone tissue engineering: an overview. J Mater Chem B. 2018;6(27):4397–4412.
[19] Midha S, Dalela M, Sybil D, et al. Advances in three-dimensional bioprinting of bone: progress and challenges. J Tissue Eng Regen Med. 2019;13 (6):925–945.
[20] Kalemtaş A, Özey N, Aydin MTA. Processing of layered porous mullite ceramics. J Aust Ceram Soc. 2018;54 (3):545–555.
[21] Hammel E, Ighodaro O-R OO. Processing and properties of advanced porous ceramics: an application based review. Ceram Int. 2014;40(10):15351–15370.
[22] Liang, X., Li, Y., Pan, L., Sang, S., Zhu, T., Li, B., Aneziris, C. G. . Preparation and enhancement of mullite reticulated porous ceramics for porous media combustion. Ceramics International. 2019;45(17):22226–22232 doi:10.1016/j.ceramint.2019.07.246
[23] Topateş G. Direct production of Si_3N_4 foams by carbothermal reduction and nitridation of SiO_2. Ceram Int. 2018;44(16):20545–20550.
[24] Mohamed Bazin M, Ahmad N, Nakamura Y. Preparation of porous ceramic membranes from Sayong ball clay. J Asian Ceram Soc. 2019;7(4):417–425.
[25] Xie B, Zhao H, Long H, et al. 3D characteristics of pores in SiC particle preforms with different starch contents by X-ray micro-computed tomography. Ceram Int. 2019;45(18):23924–23933.
[26] Chen Z, Xu G, Du H, et al. Realizable recycling of coal fly ash from solid waste for the fabrication of porous Al_2TiO_5-Mullite composite ceramic. Int J Appl Ceram Tech. 2019;16(1):50–58.
[27] Liu J, Li Y, Li Y, et al. Effects of pore structure on thermal conductivity and strength of alumina porous ceramics using carbon black as pore-forming agent. Ceram Int. 2016;42(7):8221–8228.
[28] Farahbakhsh I, Ahmadi Z, Asl MS. Densification, microstructure and mechanical properties of hot pressed ZrB_2–SiC ceramic doped with nano-sized carbon black. Ceram Int. 2017;43(11):8411–8417.

[29] Yang JF, Zhang GJ, Ohji T. Fabrication of low-shrinkage, porous silicon nitride ceramics by addition of a small amount of carbon. J Am Ceram Soc. 2001;84 (7):1639–1641.
[30] Low-Temperature KA. Sintering of Porous Ceramics Via Sodium Borate Addition. Mater Sci Res India. 2019;16 (1):48–55.
[31] Bose S, Das C. Preparation and characterization of low cost tubular ceramic support membranes using sawdust as a pore-former. Mater Lett. 2013;110:152–155.
[32] Bose S, Sawdust: DC. From wood waste to pore-former in the fabrication of ceramic membrane. Ceram Int. 2015;41(3):4070–4079.
[33] Liu -S-S, Li M, Wu J-M, et al. Preparation of high-porosity Al_2O_3 ceramic foams via selective laser sintering of Al_2O_3 poly-hollow microspheres. Ceram Int. 2020;46(4):4240–4247.
[34] Wu J-M, Zhang X-Y, Yang J-L. Novel porous Si_3N_4 ceramics prepared by aqueous gelcasting using Si_3N_4 poly-hollow microspheres as pore-forming agent. J Eur Ceram Soc. 2014;34(5):1089–1096.
[35] Wu J-M, Zhang X-Y, Xu J, et al. Preparation of porous Si_3N_4 ceramics via tailoring solid loading of Si_3N_4 slurry and Si_3N_4 poly-hollow microsphere content. J Adv Ceram. 2015;4(4):260–266..
[36] Wu JM, Zhang XY, Li JL, et al., eds. Effect of calcining temperature of Si_3N_4 poly-hollow microspheres on the properties of the porous Si_3N_4 ceramics prepared by aqueous gelcasting. Adv Sci Technol, 2014;Trans Tech Publ. DOI:10.4028/www.scientific.net/AST.88.1
[37] Caruso F, Caruso RA, Möhwald H. Nanoengineering of inorganic and hybrid hollow spheres by colloidal templating. Science. 1998;282(5391):1111–1114.
[38] Göltner CG. Porous solids from rigid colloidal templates: morphogenesis. Angew Chem. 1999;38(21):3155–3156.
[39] Sun Y, Xia Y. Shape-controlled synthesis of gold and silver nanoparticles. Science. 2002;298(5601):2176–2179.
[40] Heijnen J, Mulder A, Weltevrede R, et al. Large scale anaerobic-aerobic treatment of complex industrial waste water using biofilm reactors. Water Sci Technol. 1991;23(7–9):1427–1436.
[41] Warnock JN, Al-Rubeai M. Bioreactor systems for the production of biopharmaceuticals from animal cells. Biotechnol Appl Biochem. 2006;45(1):1–12.
[42] Cochran JK. Ceramic hollow spheres and their applications. Curr Opin Solid State Mater Sci. 1998;3 (5):474–479.
[43] Bae E, Chah S, Yi J. Preparation and characterization of ceramic hollow microspheres for heavy metal ion removal in wastewater. J Colloid Interface Sci. 2000;230(2):367–376.
[44] Klein TY, Treccani L, Rezwan K. Ceramic microbeads as adsorbents for purification technologies with high specific surface area, adjustable pore size, and morphology obtained by ionotropic gelation. J Am Ceram Soc. 2012;95(3):907–914.
[45] Li Y, Wang S, Hao P, et al. Soft-templated formation of double-shelled ZnO hollow microspheres for acetone gas sensing at low concentration/near room temperature. Sens Actuators B Chem. 2018;273:751–759.
[46] Cao J, Wang S, Zhang H, et al. Facile construction of Co_3O_4 porous microspheres with enhanced acetone gas sensing performances. Materials Science in Semiconductor Processing. 2019;101:10–15.
[47] Caruso F, Shi X, Caruso RA, et al. Hollow titania spheres from layered precursor deposition on sacrificial colloidal core particles. Adv Mater. 2001;13(10):740–744.
[48] Zhang L, Jia G, You H, et al. Sacrificial template method for fabrication of submicrometer-sized YPO_4: eu3+ hierarchical hollow spheres. Inorg Chem. 2010;49 (7):3305–3309..
[49] Li H, Ha C-S KI. Facile fabrication of hollow silica and titania microspheres using plasma-treated polystyrene spheres as sacrificial templates. Langmuir. 2008;24 (19):10552–10556.
[50] Cheow WS, Li S, Hadinoto K. Spray drying formulation of hollow spherical aggregates of silica nanoparticles by experimental design. Chem Eng Res Des. 2010;88 (5–6):673–685.
[51] Roy P, Bertrand G, Coddet C. Spray drying and sintering of zirconia based hollow powders. Powder Technol. 2005;157(1–3):20–26.
[52] Kho K, Hadinoto K. Aqueous re-dispersibility characterization of spray-dried hollow spherical silica nano-aggregates. Powder Technol. 2010;198(3):354–363.
[53] Bruinsma PJ, Kim AY, Liu J, et al. Mesoporous silica synthesized by solvent evaporation: spun fibers and spray-dried hollow spheres. Chem Mater. 1997;9 (11):2507–2512.
[54] Kempaiah DM, Yin S, Sato T. A facile and quick solvothermal synthesis of 3D microflower CeO_2 and Gd: ceO_2 under subcritical and supercritical conditions for catalytic applications. CrystEngComm. 2011;13(3):741–746.
[55] Lei S, Tang K, Yang Q, et al. Solvothermal Synthesis of Metastable γ-MnS Hollow Spheres and Control of Their Phase. Eur J Inorg Chem. 2005;2005(20):4124–4128.
[56] Ma MG, Zhu JF. Solvothermal synthesis and characterization of hierarchically nanostructured hydroxyapatite hollow spheres. Eur J Inorg Chem. 2009;2009 (36):5522–5526.
[57] Sui M, Sun X, Lou H, et al. Synthesis of hollow Fe_3O_4 particles via one-step solvothermal approach for microwave absorption materials: effect of reactant concentration, reaction temperature and reaction time. J Mater Sci. 2018;29(9):7539–7550.
[58] Wang D, Shang W, Zhang B, et al. Manganese-doped zinc oxide hollow balls for chemiresistive sensing of acetone vapors. Mikrochim Acta. 2019;186(1):44.
[59] Pan J, Zhong L, Li M, et al. Synthesis of VO_2 Hollow Spheres and Their Conversion into V_2O_5 Hollow Spheres with Improved Lithium Storage Capability. Chem–A Eur J. 2016;22(4):1461–1466.
[60] Yu J, Liu W, Yu H. A one-pot approach to hierarchically nanoporous titania hollow microspheres with high photocatalytic activity. Cryst Growth Design. 2008;8 (3):930–934.
[61] Sun X, Liu J, Li Y. Use of carbonaceous polysaccharide microspheres as templates for fabricating metal oxide hollow spheres. Chem–A Eur J. 2006;12(7):2039–2047.
[62] Wang S, Zhang J, Jiang J, et al. Porous ceria hollow microspheres: synthesis and characterization. Micropor Mesopor Mat. 2009;123(1):349–353..
[63] Liu Z, Bai H, Sun D. Facile fabrication of hierarchical porous TiO_2 hollow microspheres with high photocatalytic activity for water purification. Appl Catal B Environ. 2011;104(3):234–238.
[64] Zhou L, Zhuang Z, Zhao H, et al. Intricate hollow structures: controlled synthesis and applications in energy storage and conversion. Adv Mater. 2017;29 (20):1602914.
[65] Hong YJ, Roh KC, Lee J-K, et al. A new general approach to synthesizing filled and yolk–shell structured metal oxide microspheres by applying a carbonaceous template. Nanoscale. 2017;9(45):17991–17999.

[66] Zhao K, Cheng L, Ye F, et al. Performance of Si_3N_4 Hollow Microspheres by the Template Method and Carbothermal Reduction Nitridation. Acs Appl Mater Inter. 2019;11(42):39054–39061.
[67] Zhang S, Fan Q, Gao H, et al. Formation of Fe_3O_4@ MnO_2 ball-in-ball hollow spheres as a high performance catalyst with enhanced catalytic performances. ?J Mater Chem A. 2016;4(4):1414–1422.
[68] Wang SF, Gu F, Lü MK. Sonochemical synthesis of hollow PbS nanospheres. Langmuir. 2006;22(1):398–401.
[69] Kalemtas A. Effect of the sintering temperature on the fabrication of alumina beads. Mat. Sci. Res. India. 2019;16(2):125–135.
[70] Kimling MC, Caruso RA. Sol–gel synthesis of hierarchically porous TiO_2 beads using calcium alginate beads as sacrificial templates. J Mater Chem. 2012;22 (9):4073–4082.
[71] Chee Kimling M, Scales N, Hanley TL, et al. Uranyl-Sorption Properties of Amorphous and Crystalline TiO 2 /ZrO 2 Millimeter-Sized Hierarchically Porous Beads. Environ Sci Technol. 2012;46(14):7913–7920.
[72] Martin T, Galarneau A, Di Renzo F, et al. Morphological Control of MCM-41 by Pseudomorphic Synthesis. Angew Chem. 2002;41(14):2590–2592.
[73] Liu C, Zhang J, He Y, et al. Al_2O_3 microspheres prepared by cathode plasma electrolysis. Aus J Chem. 2017;70(1):120–124.
[74] Lai W, Chen C, Ren X, et al. Hydrothermal fabrication of porous hollow hydroxyapatite microspheres for a drug delivery system. Mater Sci Eng C. 2016;62:166–172.
[75] Liu Z, Sun DD, Guo P, et al. One-step fabrication and high photocatalytic activity of porous TiO_2 hollow aggregates by using a low-temperature hydrothermal method without templates. Chem–A Eur J. 2007;13 (6):1851–1855.
[76] Jiang W, Meng L, Zhang S, et al. Enhanced resistive acetone sensing by using hollow spherical composites prepared from MoO_3 and In_2O_3. Mikrochim Acta. 2019;186(6):359..
[77] Wu Q, Wang P, Hu S, et al. Hydrothermal synthesis of hollow silica spheres under acidic conditions. Langmuir. 2011;27(11):7185–7191.
[78] Wang H, Wang F, Liao Q, et al. Synthesis of millimeter-scale Al_2O_3 ceramic hollow spheres by an improved emulsion microencapsulation method. Ceram Int. 2015;41(3):4959–4965.
[79] Richardson K, Akinc M. Preparation of spherical yttrium oxide powders using emulsion evaporation. Ceram Int. 1987;13(4):253–261.
[80] Komeya K, Zhang C, Hotta M, et al. Hollow Beads Composed of Nanosize Ca α-SiAlON Grains. J Am Ceram Soc. 2000;83(4):995–997.
[81] Durham SJ, Shanker K, Drew RA. Carbothermal synthesis of silicon nitride: effect of reaction conditions. J Am Ceram Soc. 1991;74(1):31–37.
[82] Hnatko M, Galusek D, Šajgalík P. Low-cost preparation of Si_3N_4–SiC micro/nano composites by in-situ carbothermal reduction of silica in silicon nitride matrix. J Eur Ceram Soc. 2004;24(2):189–195.
[83] Kuskonmaz N, Sayginer A, Toy C, et al. Studies on the formation of silicon nitride and silicon carbide from rice husk. High Temp Mater Process. 1996;15 (1–2):123–128.
[84] Li X, Li R, Zhu X, et al. Properties of large-sized porous Si_3N_4 ceramic tubes fabricated by carbothermal reduction of diatomite preforms. Ceram Int. 2017;43 (13):10559–10565.
[85] Ličko T, Figusch V, Puchyova J. Synthesis of silicon nitride by carbothermal reduction and nitriding of silica: control of kinetics and morphology. J Eur Ceram Soc. 1992;9(3):219–230.
[86] Arik H, Saritas S, Gündüz M. Production of Si_3N_4 by carbothermal reduction and nitridation of sepiolite. J Mater Sci. 1999;34(4):835–842.
[87] Shan SY, Yang JF, Gao JQ, et al. Porous silicon nitride ceramics prepared by reduction–nitridation of silica. J Am Ceram Soc. 2005;88(9):2594–2596..
[88] Rahman IA, Riley FL. The control of morphology in silicon nitride powder prepared from rice husk. J Eur Ceram Soc. 1989;5(1):11–22.
[89] Sun S-Y, Wang Q, Ge -Y-Y, et al. Synthesis and growth mechanism of approximate spherical β-Si_3N_4 particles via carbothermal reduction-nitridation method. J Am Ceram Soc. 2017;100 (12):5779–5786..